

Bound states in the continuum in photonic waveguides inspired by defects

Evgeny N. Bulgakov and Almas F. Sadreev

Institute of Physics, Academy of Sciences, 660036 Krasnoyarsk, Russia

(Received 23 January 2008; revised manuscript received 2 July 2008; published 8 August 2008)

Photonic crystal with defect layer forms directed continuum for electromagnetic waves. Defect rods in the vicinity of the defect layer interact with the continuum and give rise to scattering of ingoing waves. We derive quantum-mechanical analog of the non-Hermitian Hamiltonian of the open system with complex eigenvalues, which describes a scattering of electromagnetic waves by the defect rods. In this formalism a bound state in the continuum (BIC) can be easily found by the condition that one of the complex eigenvalues becomes real for variation of dielectric constant of the defect rods. We numerically find BICs with discrete frequencies belong to the continuum for different arrangements of the defects and show that they are localized around the defects.

DOI: [10.1103/PhysRevB.78.075105](https://doi.org/10.1103/PhysRevB.78.075105)

PACS number(s): 42.70.Qs, 42.79.Gn, 41.20.Jb, 05.60.Gg

I. INTRODUCTION

In 1929, von Neumann and Wigner¹ predicted the existence of discrete solutions of the single-particle Schrödinger equation embedded in the continuum of positive-energy states. Their analysis examined by Stillinger and Herrick² was long regarded as a mathematical curiosity because of certain spatially oscillating central symmetric potentials. After it has been suggested that bound states in continuum (BIC) might be found in certain two-electron systems,^{2,3} later in 1973 Herrik⁴ and Stillinger⁵ predicted BICs in semiconductor heterostructure superlattices, which were observed by Capasso *et al.* as a very narrow absorption peak.⁶ BIC can be observed in the stationary quantum transport as a resonant state whose width tends to zero as at least one physical parameter varies continuously as it was formulated first by Friedrich and Wintgen^{7,8} in framework of a two-level model (see also Refs. 9–14). The numerical evidence for the BIC in straight waveguide with an attractive finite-size impurity was presented by Kim *et al.*¹⁵ for the variation of the impurity size. Furthermore, calculations in microwave and semiconductor open structures showed that the resonance width also can turn to zero for variation of angle of bent waveguide,¹⁶ shape of quantum dot and microwave resonator,^{14,17} or magnetic field.¹⁸

The underlying simple mechanism of the BIC phenomenon can be demonstrated using the idea of perfect reflections in the Fabry-Perot resonator.¹⁹ The total transmission amplitude can be easily calculated as a geometrical sum over all individual transmitted and reflected elementary processes. This gives the simple expression $T = t^2 / (1 - r^2 e^{2ikL})$ for the transmission probability, where t and r are the complex amplitudes of the transmission and reflection, respectively, for individual processes and k is the wave number. The bound states are defined by the zeros of the denominator in T , i.e., by $\sin[\phi(E) + \pi q(E)L] = 0$, where $\phi(E) = \arg(r)$. One obtains therefore a quantization rule for the particle trapped in the space between the mirrors in the Fabry-Perot resonator of the length L . The Fabry-Perot approach was explored for two identical billiards connected by a wire^{17,20,21} and recently for two parallel dielectric gratings and two arrays of thin parallel dielectric cylinders in photonic crystal.²²

For the considered case of the photonic waveguide coupled to defects (see below Fig. 4) the Fabry-Perot ap-

proach is hardly applicable because of an interaction between the defects. However, to restrict ourselves by two defects, we can use the two-level approximation for description of the defects.^{9–12} By tuning the dielectric constant of the defects, we can perform the crossing of resonances. For that process we have strong interference of resonances,⁷ which might result in complete suppression of the coupling of the resonance state with the continuum^{11–14,23} to convert the state into the BIC. Recently it was rigorously shown that it is exactly equivalent to the resonance width equaled to zero.^{18,24}

At least, the following conditions are necessary for experimental observation of BICs. The possibility of continual variation of spectrum of the closed system, the high quality of whole open system, and each continuum has to support one open channel (the single-channel transport). The open microwave billiards with movable wall and the quantum dots with variable confined potential can satisfy to these conditions.¹⁴ The goal of the present paper is to show that photonic crystal (PC) with defect layer with additional defects in the vicinity of the layer might be a candidate for the study of BICs.

Compared to homogeneous media, the existence of band gaps inside Bloch bands, where linear light propagation is forbidden, forms a new feature in periodic media of PC.^{25,26} To be specific we consider the square lattice (lattice constant a) of cylindrical dielectric rods of radius $r_{\text{rod}} = 0.18a$ and dielectric constant $\epsilon = 11.56$ in air as given in Refs. 27 and 28. The background bulk PC exhibits a TM-polarization (the electric field is parallel to the axis of the cylinder) band gap at $0.302 \leq \omega \leq 0.444$ (Ref. 27) in units of $2\pi c/a$, where c is the light speed in vacuum. Removing a row of rods creates the single mode PC waveguide with effective width of order of a few a .^{27–32} The waveguide supports a single wide band of guided mode spanning from 0.312 to the upper band edge. The dispersion relation of the propagating guided mode is shown in Fig. 10(b) of Ref. 27. Therefore such a PC forms the directed continuum of TM electromagnetic field.^{25,26}

In the framework of the Feshbach's theory of resonances, Friedrich and Wintgen⁷ have shown that BIC occurs due to the interference of resonances for their crossing. Therefore the simplest PC system which might demonstrate such a phenomenon consists of, at least, the single mode PC waveguide side coupled to two defects or two single mode cavities. The system was considered as a realization of model³³ in PC,^{28,34}

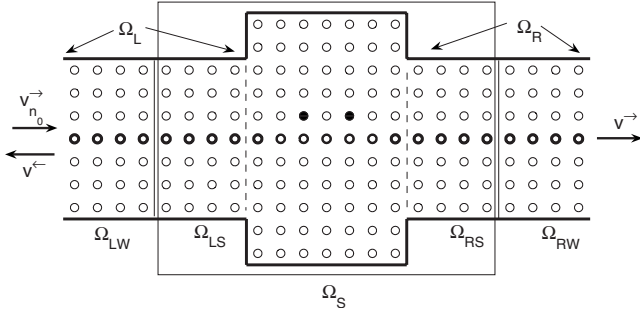


FIG. 1. PC consists of a square lattice of dielectric rods ($\epsilon=11.56$) of radius $0.18a$ in air. The defect rods of the same radius but with different $\epsilon=1$ (air) in PC shown by bold circles define the left and right waveguides. Filled circles show additional local defect rods with variable dielectric constant ϵ_d which gives rise to scattering of propagating mode in the left and right waveguides. The scattering region Ω_S includes an area of local defects as parts of waveguides Ω_{LS} and Ω_{RS} . Frame shows all rods involved for the calculation of the transmission.

as well as by the solution of the Maxwell equations.³⁵ Moreover that system is similar to the double dot system which was considered in many publications to demonstrate BICs.^{9,13,17,20,21} The total system is shown in Fig. 1 where two interacting defect rods shown by filled circles are coupled with the photonic continuum.

In Fig. 2 we show the frequency of electromagnetic field varies dependent on the dielectric constant of single isolated defect cylinder. Next Fig. 3 demonstrates that this electromagnetic field is localized in the vicinity of the defect rod.

In order to consider the BICs we solve the Maxwell equations for the TM mode in the PC with defect rods by expansion of electromagnetic field over maximally localized photonic Wannier functions.^{27,36} As a result we formulate the effective model on a squared lattice and derive the non-Hermitian effective Hamiltonian of the open system with complex eigenvalues.¹⁸ Then BIC can be easily found by the condition that at least one of the complex eigenvalues becomes real.^{18,24}

II. LATTICE MODEL DESCRIBED LIGHT TRANSMISSION IN THE DEFECT PC

In the present section we borrow notations from the review by Busch *et al.*²⁷ The description of defect structures

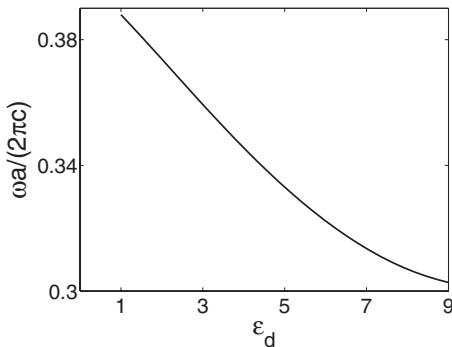


FIG. 2. The frequency of isolated bound mode for the single isolated defect cylinder as dependent on its dielectric constant ϵ_d .

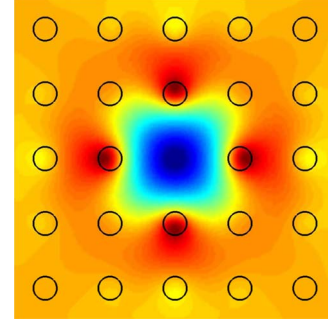


FIG. 3. (Color online) Pattern of localized solution for electromagnetic field of the isolated defect cylinder for a frequency taken from Fig. 2. The pattern very slowly changes with variation of this frequency.

embedded in the PC starts with the wave equation for the TM mode of electromagnetic field:

$$\left\{ \nabla^2 + \frac{\omega^2}{c^2} [\epsilon(\mathbf{r}) + \delta\epsilon(\mathbf{r})] \right\} E(\mathbf{r}) = 0, \quad \epsilon(\mathbf{r} + \mathbf{R}) = \epsilon(\mathbf{r}), \quad (1)$$

where $\mathbf{R} = a(j\mathbf{e}_x + m\mathbf{e}_y)$ runs over cells of a square lattice of rods. $\mathbf{e}_x, \mathbf{e}_y$ are the unit vectors of the square lattice. The dielectric constant is considered to be $\epsilon(\mathbf{r}) = \epsilon$ inside the rods and unit outside. Because of the Bloch-Floquet theorem the solution of Eq. (1) can be written as $E_{n\mathbf{k}}(\mathbf{r} + \mathbf{R}) = \exp(i\mathbf{k}\mathbf{R})E_{n\mathbf{k}}(\mathbf{r})$ where the index n enumerates the Bloch bands with the following normalization

$$\int d^2\mathbf{r} E_{n\mathbf{k}}^*(\mathbf{r}) \epsilon(\mathbf{r}) E_{n'\mathbf{k}'}(\mathbf{r}) = \delta_{nn'} \delta(\mathbf{k} - \mathbf{k}'). \quad (2)$$

The photonic Wannier functions $W_{n\mathbf{R}}$ are defined through a lattice Fourier transform

$$W_{n\mathbf{R}}(\mathbf{r}) = \frac{V_{\text{WSC}}}{(2\pi)^2} \int_{\text{BZ}} d^2\mathbf{k} \exp(-i\mathbf{k}\mathbf{R}) E_{n\mathbf{k}}(\mathbf{r}), \quad (3)$$

of the Bloch functions, $E_{n\mathbf{k}}(\mathbf{r})$. Here, V_{WSC} denotes the volume of the Wigner-Seitz cell. The photonic Wannier function $W_{n\mathbf{R}}$ has the frequency range covered by band n . Because of the translational invariance $W_{n\mathbf{R}}(\mathbf{r}) = W_{n0}(\mathbf{r} - \mathbf{R})$. Moreover the photonic Wannier functions obey the following normalization condition:

$$\int d^2\mathbf{r} W_{n\mathbf{R}}^*(\mathbf{r}) \epsilon(\mathbf{r}) W_{n'\mathbf{R}'}(\mathbf{r}) = \delta_{nn'} \delta_{\mathbf{R}\mathbf{R}'}. \quad (4)$$

However these Wannier functions are poorly localized. Marzari and Vanderbilt³⁶ (see also Ref. 27) proposed an efficient scheme for the computation of maximally localized Wannier functions by a superposition of the Bloch solutions $E_{n\mathbf{k}}(\mathbf{r})$ from N_W different bands,

$$E_{n\mathbf{k}}(\mathbf{r}) \rightarrow \sum_{m=1}^{N_W} U_{mn}(\mathbf{k}) E_{m\mathbf{k}}(\mathbf{r}). \quad (5)$$

The matrix elements of transformation $U_{mn}(\mathbf{k})$ are found numerically by minimization of an appropriate spread functional,

$$\Omega = \sum_n [\langle n\mathbf{0}|r^2|n\mathbf{0}\rangle - \langle n\mathbf{0}|\mathbf{r}|n\mathbf{0}\rangle^2], \quad (6)$$

$$\langle n\mathbf{R}|f(\mathbf{r})|n'\mathbf{R}'\rangle = \int d^2\mathbf{r} W_{n\mathbf{R}}^*(\mathbf{r}) W_{n'\mathbf{R}'}(\mathbf{r}) \epsilon(\mathbf{r}) f(\mathbf{r}). \quad (7)$$

The defect rods in the PC are presented in Eq. (1) by a change of the dielectric constant $\delta\epsilon(\mathbf{r})$. In particular if to arrange defect rods into a chain, then

$$\delta_W\epsilon(\mathbf{r}) = (\epsilon_W - \epsilon) \sum_{m=-\infty}^{\infty} \Theta(\mathbf{r} - \mathbf{R}_m). \quad (8)$$

This chain forms guided waveguide for the light and is shown in Fig. 1 by bold circles. $\Theta(\mathbf{r})$ defines the area of the defect rod, $\Theta(\mathbf{r})=1$ inside a defect rod and $\Theta(\mathbf{r})=0$ outside. Moreover we introduce additional N_d defect rods as shown in Fig. 1 by filled circles,

$$\delta_S\epsilon(\mathbf{r}) = \sum_{d=1}^{N_d} (\epsilon_d - \epsilon) \Theta(\mathbf{r} - \mathbf{R}_d), \quad (9)$$

where the dielectric constants ϵ_d are assumed can vary. The subscripts W and S in formulas (8) and (9) mean waveguide and scattering defects.

After expansion of electric field over the maximally localized Wannier functions $E(\mathbf{r}) = \sum_{n\mathbf{R}} E_{n\mathbf{R}} W_{n\mathbf{R}}(\mathbf{r})$ the basic Eq. (1) becomes²⁷

$$\sum_{n'\mathbf{R}'} \left[\delta_{nn'} \delta_{\mathbf{R}\mathbf{R}'} + D_{\mathbf{R}\mathbf{R}'}^{nn'} - \left(\frac{c}{\omega}\right)^2 A_{\mathbf{R}\mathbf{R}'}^{nn'} \right] E_{n'\mathbf{R}'} = 0, \quad (10)$$

$$A_{\mathbf{R}\mathbf{R}'}^{nn'} = \frac{V_{\text{WSC}}}{(2\pi)^2} \int_{\text{BZ}} d^2\mathbf{k} e^{i\mathbf{k}(\mathbf{R}-\mathbf{R}')} \sum_m U_{nm}^+(\mathbf{k}) \left(\frac{\omega_{m\mathbf{k}}}{c}\right)^2 U_{mn'}(\mathbf{k}),$$

$$D_{\mathbf{R}\mathbf{R}'}^{nn'} = \int d^2\mathbf{r} W_{n\mathbf{R}}^*(\mathbf{r}) [\delta_W\epsilon(\mathbf{r}) + \delta_S\epsilon(\mathbf{r})] W_{n'\mathbf{R}'}(\mathbf{r}). \quad (11)$$

Here $\omega_{m\mathbf{k}}$ are the photonic dispersion relations with respect to the wave vector \mathbf{k} in ideal PC. V_{WSC} denotes the volume of the Wigner-Seitz cell. The matrix elements $A_{\mathbf{R}\mathbf{R}'}^{nn'}$ and $D_{\mathbf{R}\mathbf{R}'}^{nn'}$ are real and rapidly decay with growth of $|\mathbf{R}-\mathbf{R}'|$.

III. EFFECTIVE HAMILTONIAN FOR PHOTONICS

Among many other quantum mechanical concepts there is a non-Hermitian effective Hamiltonian which describes open system. The concept is based on the Feshbach projection operator technique³⁷ (see also Ref. 38). In this formalism, the whole function space is divided into two subspaces that are coupled with one another. Discrete states localized inside of closed system form one of the subspaces while the continuum of extended propagating solutions of waveguide are responsible for the outer subspace. Then projection of the Hamilton operator of the whole system $H = H_B + \sum_C (H_C + V_{BC} + V_{CB})$ onto the space of discrete states of the closed system formulates the effective Hamiltonian,^{37,39-42}

$$H_{\text{eff}} = H_B + \sum_C V_{BC} \frac{1}{E^+ - H_C} V_{CB}. \quad (12)$$

Here H_B is the Hamiltonian of the closed system, V_{BC} and V_{CB} stand for the coupling matrix elements between the eigenstates of H_B and the waveguides that may consist of different continua C , and E is the energy of scattering particle. The term $E^+ = E + i0$ ensures that only outgoing waves will be present in the exit continua. As a result the effective Hamiltonian (12) is non-Hermitian whose complex eigenvalues z_λ of the effective Hamiltonian determine the positions as $\text{Re}(z_\lambda)$ and widths of the resonance states as $-2 \text{Im}(z_\lambda)$. For the limit $\text{Im}(z_\lambda) \rightarrow 0$ the corresponding eigenfunction of H_{eff} is becoming the BIC localized interior of the closed system.^{18,24}

Our aim then is to formulate the non-Hermitian effective Hamiltonian for the PC waveguide coupled to the defects. The particular case of that system is shown in Fig. 1. There are two defect cylinders shown by filled circles that are coupled to the propagating TM mode in the waveguide of PC shown by bold circles. The direct way to derive the effective Hamiltonian would be calculation of matrix elements of coupling operators in Eq. (12). This way in the tight-binding approach is given in Refs. 43 and 44. However, in the PC we cannot restrict ourselves by the hopping matrix elements between the nearest neighbors only. Moreover each site is presented by the four Wannier states. The coupling of the Wannier functions is relevant at the distances between rods till $4a$.²⁷ That also agrees with our numerical practice. As a result, in the PC we obtain the two-dimensional lattice model shown in Fig. 1 instead of simple tight-binding model coupled to aside defects.^{44,45} The coupling matrix is to be calculated in regions labeled in Fig. 1 as Ω_C , where $C = L, R$. Therefore the calculation of the coupling matrix in Eq. (12) is formidable task as different from the tight-binding models in quantum mechanics.^{43,44}

Here we use a different approach to formulate the effective Hamiltonian based on the Ando scattering theory in wires⁴⁶ generalized for the present case of the PC. Let us first briefly outline the Ando's approach for the one-dimensional tight-binding model⁴⁶ for the reader's convenience. The model consists of the N -site wire coupled to the ideal semi-infinite tight-binding wires (leads), left and right, via the coupling constant v :

$$H = - \sum_{j=-\infty}^{\infty} t_j |j\rangle \langle j+1| + \text{H.c.}, \quad (13)$$

where $t_j=1$ everywhere, except $t_0=t_N=v$. In the left ideal wire the solutions are composed of the right-going (incident) $\exp(ikja)$ and left-going (reflected) $r \exp(-ikja)$ solutions. Here r is the amplitude of reflection. Therefore, the amplitude of wave function at the utmost right point $j=0$ is

$$\psi_0 = \psi_0^+ + \psi_0^-. \quad (14)$$

Then the solution at the nearest site $j=-1$ can be written as follows:⁴⁶

$$\psi_{-1} = F_{\leftarrow}^{-1}\psi_0 + [F_{\leftarrow}^{-1} - F_{\leftarrow}^{-1}]\psi_0^{\rightarrow}, \quad (15)$$

where for the one-dimensional tight-binding chain $F_{\leftarrow} = \exp(-ika)$ and $F_{\rightarrow} = \exp(ika)$. On the other right wire only right-going (outgoing) wave exist at site $N+1$. Therefore,

$$\psi_{N+2} = F_{\rightarrow}\psi_{N+1}. \quad (16)$$

Consequently writing the Schrödinger equation for $\psi_0, \psi_1, \dots, \psi_N, \psi_{N+1}$ we can complete the system equations and obtain the Green's function, which defines the transmission from site 0 to site $N+1$:

$$G(E) = \frac{1}{E^+ - H_{\text{eff}}}, \quad (17)$$

with the matrix of rank $N+2$,

$$H_{\text{eff}} = \begin{bmatrix} -\exp(ika) & -v & 0 & \dots & 0 & 0 \\ -v & 0 & -1 & \dots & 0 & 0 \\ 0 & -1 & 0 & \dots & 0 & 0 \\ \vdots & \vdots & \vdots & \ddots & \vdots & \vdots \\ 0 & 0 & 0 & \dots & 0 & -v \\ 0 & 0 & 0 & \dots & -v & -\exp(ika) \end{bmatrix}. \quad (18)$$

The effective Hamiltonian (18) is not Hermitian because of terms $\exp(ika)$ resulted by that the wave $\exp(ikaj)$ incidents from the left of wire.

It is important that Ando presented the case of two-dimensional tight-binding wire consisted of M lattice sites in the direction orthogonal to the transport axis. Then the solution at the j th slice of the wire is Ψ_j consisting of M sites obeyed to

$$\Psi_j = \lambda \Psi_{j-1}. \quad (19)$$

At the slice $j=0$ there are the M left-going solutions $U^{\leftarrow} = (\Psi_1^{\leftarrow}, \Psi_2^{\leftarrow}, \dots, \Psi_M^{\leftarrow})$ corresponding to $\lambda_1^{\leftarrow}, \lambda_2^{\leftarrow}, \dots, \lambda_M^{\leftarrow}$ and the M right-going solutions $U^{\rightarrow} = (\Psi_1^{\rightarrow}, \Psi_2^{\rightarrow}, \dots, \Psi_M^{\rightarrow})$ corresponding to $\lambda_1^{\rightarrow}, \lambda_2^{\rightarrow}, \dots, \lambda_M^{\rightarrow}$. Relations (14)–(16) remain the same however with

$$F_s = U_s \Lambda_s U_s^{-1}, s = \begin{cases} \rightarrow \\ \leftarrow \end{cases}, \quad (20)$$

where Λ_s is the diagonal matrix consisted of eigenvalues $\lambda_1^s, \lambda_2^s, \dots, \lambda_M^s$. The corresponding matrix of the effective Hamiltonian acquires the rank $(N+2) \times M$ and is given in Ref. 46.

Now we can apply the described derivation of the effective Hamiltonian to the PC structure shown in Fig. 1. Similar to the tight-binding leads we have the one-dimensional periodicity of the waveguides. The only difference is that the number of hopping matrix elements substantially exceeds unit. Let us write the solution in the left waveguide in the same form as it is given in Eq. (14), i.e., superposed of incident and reflected waves. Correspondingly in the right waveguide we have only transmitted wave. These solutions are to be matched with unknown solution in the scattering region labeled in Fig. 1 by Ω_S . The matching is performed in

the regions $\Omega_{CW} \cup \Omega_{CS}$, where $C=L, R$. We present the basic Eq. (10) for a whole PC as

$$\hat{H}(\omega)\Psi = 0,$$

with matrix elements of the ‘‘Hamiltonian’’ operator given by expression in round parentheses and the state Ψ is a row vector of amplitudes E_{nR} . This equation presents the equation for the eigenvector Ψ and eigenfrequencies defined by $\text{Det}[\hat{H}(\omega)] = 0$. We decompose the operator \hat{H} as follows:

$$(\hat{H}_B + \hat{V}_L + \hat{V}_R + \hat{H}_{\text{out}})\Psi = 0, \quad (21)$$

where \hat{H}_B involves all couplings inside the scattering region Ω_S , $\hat{V}_C, C=L, R$ describe couplings of the scattering region with external one Ω_{out} , and \hat{H}_{out} includes all couplings in the region Ω_{out} . The region Ω_{out} comprises all rods beyond Ω_S and includes in particular the regions Ω_{CW} as parts of waveguides. The photonic eigenmodes labeled by integers p in semi-infinite waveguides consist of propagating and decaying (evanescent) waves, right-going v_p^{\rightarrow} and left-going v_p^{\leftarrow} . Moreover we assume that the mode p_0 incidents from the left waveguide which scatters onto reflected and transmitted p modes. These modes are calculated numerically in Refs. 27 and 47 and shown in book.²⁹ The solutions are given at each slice perpendicular to the waveguide axis by the vector of dimension $N_W \times N_R$. Here N_W is a number of Wannier functions and N_R is a finite number of lattice sites, surrounding defect rods inside each slice including the defect rod, for which the coupling of Wannier functions is relevant. Specifically, as shown in Fig. 1 $N_R=7$. Then, each guided photonic mode is given by the dispersion relation associated with the wave vector $k_p(\omega)$, where $p=1, \dots, 2N_W N_R L$ and L is the distance above which the coupling between slices can be neglected. We consider that only one photonic mode p_0 is propagating while other are evanescent. As shown in Fig. 1 a length of buffer region $\Omega_{CW} \cup \Omega_{CS}$ is just $2L$ taken equal to eight.

Next, similar to Eq. (19) we write the relations which connect the regions Ω_{CW} of the waveguides with the regions Ω_{CS} of the scattering region,²⁷

$$\begin{aligned} v_p^{\leftarrow}(\Omega_{LS}) &= \lambda_p v_p^{\leftarrow}(\Omega_{LW}), \\ v_p^{\rightarrow}(\Omega_{RW}) &= \lambda_p v_p^{\rightarrow}(\Omega_{RS}), \\ v_p^{\leftarrow}(\Omega_{LW}) &= \Lambda_p v_p^{\leftarrow}(\Omega_{LS}), \\ v_p^{\leftarrow}(\Omega_{RS}) &= \Lambda_p v_p^{\leftarrow}(\Omega_{RW}), \end{aligned} \quad (22)$$

where $\lambda_p = \exp[-k_p(\omega)a]$, $\Lambda_p = \exp[k_p(\omega)a]$, $\lambda_{p_0} = \exp[ik_{p_0}(\omega)a]$, and $\Lambda_{p_0} = \exp[-ik_{p_0}(\omega)a]$.²⁷

Let us, first, consider a matching at the right buffer region $\Omega_{RS} \cup \Omega_{RW}$ where only the outgoing modes v_p^{\rightarrow} exist. If there is some superposition of the modes in the region Ω_{RS} ,

$$v^{\rightarrow}(\Omega_{RS}) = \sum_{p=1}^N a_p v_p^{\rightarrow}(\Omega_{RS}), \quad (23)$$

then we have the following superposition in the next region Ω_{RW} because of relations (22)

$$v^{\rightarrow}(\Omega_{RW}) = \sum_{n=1}^N a_p \lambda_p v_p^{\rightarrow}(\Omega_{RS}), \quad (24)$$

where $N=2N_w N_R L$ is a total number of photonic modes in the waveguide (the number of continua). Introduce square matrices

$$\hat{U}_{\rightarrow} = [v_1^{\rightarrow}(\Omega_{RS}), v_2^{\rightarrow}(\Omega_{RS}), \dots, v_N^{\rightarrow}(\Omega_{RS})],$$

and the row vector $A^T = (a_1, a_2, \dots, a_N)$. Then from Eq. (23) we have

$$A = \hat{U}_{\rightarrow}^{-1} v^{\rightarrow}(\Omega_{RS}).$$

Correspondingly from Eq. (24), we obtain

$$v^{\rightarrow}(\Omega_{RW}) = \hat{T}_{\rightarrow} v^{\rightarrow}(\Omega_{RS}) = \hat{U}_{\rightarrow} \hat{\Lambda} \hat{U}_{\rightarrow}^{-1} v^{\rightarrow}(\Omega_{RS}), \quad (25)$$

where $\hat{\Lambda}$ is the diagonal matrix consisted of eigenvalues λ_p . Similar relations can be written for v^{\leftarrow} with a difference that matrix \hat{U}_{\leftarrow} consists of the modes $v_p^{\leftarrow}(\Omega_R)$.

The right buffer region Ω_R consists of the region Ω_{RS} , a part of the scattering region, and Ω_{RW} , the part of the right waveguide. Therefore, the operator \hat{H} decomposes in this region as follows:

$$\hat{H}(\Omega_R) = \begin{pmatrix} \hat{H}_{RS} & \hat{V}_{SW} \\ \hat{V}_{SW}^{\dagger} & \hat{H}_{RW} \end{pmatrix}. \quad (26)$$

According to Eq. (25) the solution in the region Ω_R can be written as

$$v^{\rightarrow}(\Omega_R) = \begin{bmatrix} v^{\rightarrow}(\Omega_{RS}) \\ \hat{T}_{\rightarrow} v^{\rightarrow}(\Omega_{RS}) \end{bmatrix}. \quad (27)$$

Therefore, with account of Eq. (26) we have

$$\hat{H}(\Omega_R) v^{\rightarrow}(\Omega_R) = \hat{H}_{\text{eff},R} v^{\rightarrow}(\Omega_{RS}),$$

where

$$\hat{H}_{\text{eff},R} = \hat{H}_{RS} + \hat{V}_{SW} \hat{T}_{\rightarrow}. \quad (28)$$

In the left buffer region Ω_L the solution consists of the incident and reflected waves $v(\Omega_L) = v_{p_0}^{\rightarrow}(\Omega_L) + v^{\leftarrow}(\Omega_L)$. Because of equation similar to Eq. (27) it takes the following form:

$$v(\Omega_L) = v_{p_0}^{\rightarrow}(\Omega_L) + \begin{bmatrix} \hat{T}_{\leftarrow} v^{\leftarrow}(\Omega_{LS}) \\ v^{\leftarrow}(\Omega_{LS}) \end{bmatrix}, \quad (29)$$

where $\hat{T}_{\leftarrow} = \hat{U}_{\leftarrow} \hat{\Lambda} \hat{U}_{\leftarrow}^{-1}$, where $\hat{\Lambda} = \text{diag}(\Lambda_p)$. Then

$$\begin{aligned} v(\Omega_L) &= \hat{T}_{\rightarrow}^{-1} v_{p_0}^{\rightarrow}(\Omega_{LS}) + \hat{T}_{\leftarrow} v^{\leftarrow}(\Omega_{LS}) \\ &= (\hat{T}_{\rightarrow}^{-1} - \hat{T}_{\leftarrow}) v_{p_0}^{\rightarrow}(\Omega_{LS}) + \hat{T}_{\leftarrow} v(\Omega_{LS}). \end{aligned} \quad (30)$$

Similar to Eq. (26) we write the operator H in the left buffer region $\Omega_L = \Omega_{LW} \cup \Omega_{LS}$ as follows:

$$\hat{H}(\Omega_L) = \begin{pmatrix} \hat{H}_{LW} & \hat{V}_{WS}^{\dagger} \\ \hat{V}_{WS} & \hat{H}_{LS} \end{pmatrix}. \quad (31)$$

Consequently one can write

$$\begin{aligned} \hat{H}(\Omega_L) v(\Omega_L) &= \hat{H}(\Omega_L) \begin{bmatrix} v(\Omega_{LW}) \\ v(\Omega_{LS}) \end{bmatrix} \\ &= \hat{H}_{LS} v(\Omega_{LS}) + \hat{V}_{WS} (\hat{T}_{\rightarrow}^{-1} - \hat{T}_{\leftarrow}) v_{p_0}^{\rightarrow}(\Omega_{LS}). \end{aligned} \quad (32)$$

Finally from Eqs. (28) and (32) we obtain the closed equation for the vector of state Ψ mapped onto interior the scattering region Ω_S . This equation takes the following form

$$\hat{H}_{\text{eff}} \Psi = -V_{WS} (\hat{T}_{\rightarrow}^{-1} - \hat{T}_{\leftarrow}) v_{p_0}^{\rightarrow}(\Omega_{LS}), \quad (33)$$

$$\hat{H}_{\text{eff}}(\omega) = \hat{H}_B(\omega) + V_{SW} \hat{T}_{\rightarrow}(\omega) + V_{WS} \hat{T}_{\leftarrow}(\omega), \quad (34)$$

with account of Eqs. (26)–(28). Equation (33) is equivalent to the Lippman-Schwinger equation in quantum mechanics. In the last case the scattering wave function inside the scattering region obeys the following equation:^{18,39,40,44}

$$(H_{\text{eff}} - E) |\psi_S\rangle = V_{BL} |E, L\rangle, \quad (35)$$

provided that a quantum particle incidents from the left at the state $|E, L\rangle$. V_{BL} is the coupling matrix between lead L and dot B . There is however an important difference between the quantum case and photonic one. A free parameter, the energy of incident quantum particle, is separated in the left hand of the Lippman-Schwinger Eq. (35). For the PC case the free parameter, frequency ω of incident wave, is the argument of all operators in Eq. (34). The right hand of Eq. (33) shows that the guided photonic mode p_0 is the source of light interior the scattering region, i.e., in the vicinity of the defect rods. Solution Ψ of Eq. (33) can be expressed via the Green function which is an inverse of the operator $\hat{H}_{\text{eff}}(\omega)$. As in quantum mechanics the scattering boundary condition that ingoing wave scatters onto outgoing waves gives rise to that the operator $\hat{H}_{\text{eff}}(\omega)$ is non-Hermitian. Its complex eigenvalues $z(\omega)$ have a simple physical context: $\text{Re}[z(\omega_m) + \omega_m]$ give the positions of resonances ω_m and $\Gamma_m = -2 \text{Im}[z(\omega_m)]$ do their widths in the wave transmission provided that the fix point equation $\omega_m = \text{Re}[z(\omega_m)] + \omega_m$ is fulfilled.⁴¹ Therefore, for PC the positions of resonances are given by equation $\text{Re}[z(\omega_m)] = 0$. Except some simple cases this nonlinear fix point equation can be solved only numerically.

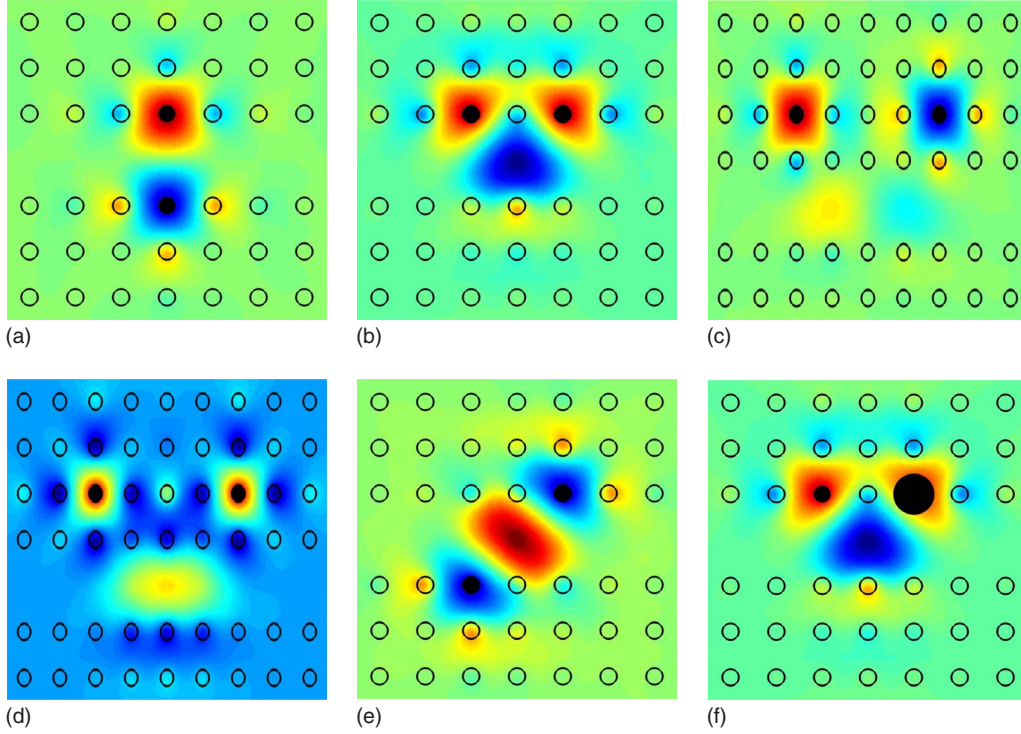


FIG. 4. (Color online) Examples of BICs for different arrangements of the defect rods with radii $r_{\text{rod}}=0.18a$ and $\epsilon=11.56$. (a) The defects are disposed perpendicular to the waveguide. The BIC state odd relative to the transport axis for the parameters $\omega a/2\pi c=0.3557$ and $\epsilon_d=2.7406$. (b)–(d) The defects are disposed parallel to the waveguide. (b) The BIC state even relative to the axis perpendicular to the transport axis for parameters $\omega a/2\pi c=0.3753$ and $\epsilon_d=3.086$. (c) The odd BIC for $\omega a/2\pi c=0.3751$ and $\epsilon_d=1.9634$. (d) The even BIC for $\omega a/2\pi c=0.3279$ and $\epsilon_d=5.5642$. (e) The even BIC symmetrical relative to inversion of coordinates $x \rightarrow -x$ and $y \rightarrow -y$ for $\omega a/2\pi c=0.3752$ and $\epsilon_d=2.5646$. (f) The case of different defect rods with $r_{\text{rod}}=0.18a$ (left) and $r_{\text{rod}}=0.45a$ (right) for $\omega a/2\pi c=0.3745$ and $\epsilon_{d1}=0.8576$; $\epsilon_{d2}=3.1348$.

As shown in Ref. 18, BIC Ψ_s , as a peculiar solution of the Lippman-Schwinger equation $\hat{H}_{\text{eff}}(\omega_s)\Psi_s=0$ localized in the scattering region, occurs in particular case of singular matrix $\hat{H}_{\text{eff}}(\omega_s)^{-1}$. Therefore, we can formulate the equation for BIC as follows:

$$\det \hat{H}_{\text{eff}}(\omega_s) = 0. \quad (36)$$

From the equation for the eigenvalues and right eigenvectors

$$\hat{H}_{\text{eff}}(\omega)|z_\lambda(\omega) = z_\lambda(\omega)|z_\lambda(\omega), \quad (37)$$

we can rewrite Eq. (36) as $\Pi_\lambda z_\lambda(\omega_s)=0$. This equation is equivalent to statement that, at least, one of the eigenvalues of the matrix $H_{\text{eff}}(\omega)$ is to be zero at $\omega=\omega_s$, i.e.,

$$z_{\lambda_0}(\omega_s) = 0. \quad (38)$$

Equation (38) shows that the resonance width as $-2 \text{Im}[z(\omega_s)]$ equals to zero, i.e., the BIC, on the one hand. On the other hand, it does the frequency ω_s of the BIC by the equation $\text{Re}[z_{\lambda_0}(\omega_s)]=0$. In order to achieve this condition which is the necessary and sufficient one for BIC to exist, an additional physical parameter is to be free.⁷ We take here that the dielectric constant of the defect rods ϵ_d can be varied. If the eigenvector Ψ_s of matrix $H_{\text{eff}}(\omega_s)$ is orthogonal to the right-hand state in Eq. (33), then the solution of the Eq. (33) becomes superposed;

$$\Psi = \alpha\Psi_s + \Psi_p. \quad (39)$$

Here Ψ_s is the localized BIC, Ψ_p is particular extended solution of the Lippmann-Schwinger Eq. (33), and α is arbitrary factor. Therefore, at the BIC point the solution becomes degenerated.

The rank of the matrix \hat{H}_{eff} equals number of sites in the region Ω_s multiplied by the number of the Wannier functions Eq. (4). Therefore Eqs. (33) and (36), complemented by the fix point equation, and $\hat{H}_{\text{eff}}(\omega_s)\Psi_s=0$ can be solved only numerically. First, we show in Figs. 4(a)–4(e) examples of BICs for different arrangements of the defect rods in vicinity of the waveguide including the case of different defect rods Fig. 4(f). For better illustration of the space profile of BIC we complement Fig. 4 by three-dimensional (3D) plot for particular case of the different defect rods. One can see from Figs. 4 and 5 that the BICs are mostly localized in the defect rods however with inclusion of neighbors. Figures 4(c) and 4(d) demonstrate odd and even BICs respectively for the same structure of the defect rods in PC.

An example of the extended solution Ψ_p is shown in Fig. 6 (inset) which describes the transport behavior of EM wave in the vicinity of the BIC point.

Similar to the open quantum dots¹⁴ the line of maximal transmission touches the line of the zero transmission at the BIC point as shown in Fig. 7. The transmission probability is

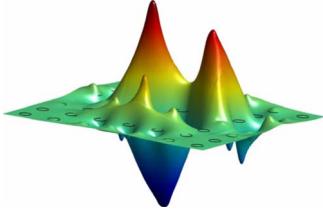


FIG. 5. (Color online) 3d plot of BIC for the case in Fig. 4(f). It is shown that BIC is asymmetric because of different defect rods.

defined as $T = |a_{p_0}|^2$ where a_{p_0} is the coefficient of expansion of solution in the right waveguide over the right-going waves Eq. (23). The phenomenon that in a vicinity of the BIC point the Breit-Wigner resonance and Fano line shape appear in the same energy window was found numerically by Kim *et al.*¹⁵ Moreover for the limit to the BIC point the Fano resonance is collapsed^{15,16} as one can follow up from Figs. 6 and 7. Analytically, the collapse of the Fano resonance for an approaching to the BIC point was considered in the two-level approximation.^{14,18} In the very vicinity of the BIC point whether the transmission is unit or zero crucially depends on a way to approach the BIC point in the parametric space of frequency and dielectric constant of the defect rods ϵ_d . Similar, the superposition coefficient α in Eq. (39) does. Figure 6 shows the transmission probability for the particular case of two choices of the dielectric constant of the defect rods and demonstrates collapse of the Fano resonances.

IV. SUMMARY

The typical scattering problem considers a wave which incidents and scatters by some local inhomogeneity. For the present case of the photonic crystal with defect layer the former is the EM wave which can propagate without change

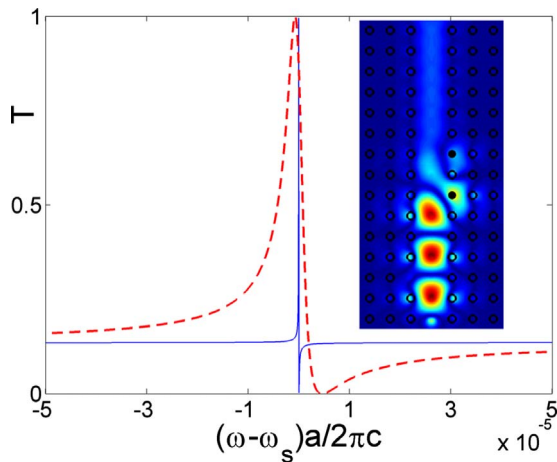


FIG. 6. (Color online) The probability of transmission of propagating photonic mode as dependent on the frequency in the vicinity of BIC shown in Fig. 4(b) for two sets of the dielectric constant of the defect rods $\omega_s = 0.3753$, $\epsilon_{d1} = 3.08351791$, $\epsilon_{d2} = 3.088568$ (solid line), $\epsilon_{d1} = 3.06331$, and $\epsilon_{d2} = 3.10877$ (dashed line). BIC appears for $\epsilon_{d1} = \epsilon_{d2} = 3.08604$. The inset right shows pattern of transport solution Ψ_p at this point.

of shape. The frequency of the wave fills some continual band forming a continuum of the Hilbert states. An inclusion of the additional defects in the vicinity of the defect layer gives rise to scattering of the incident waves. A knowledge of solution for the incident and reflected waves allows us to reduce the full Hilbert space to the finite number of states which describe only the scatterer. There are two ways to achieve that. The first is the N -level Friedrichs-Fano approach for that BIC can be diagnosed by a square integrable condition^{1,2,7,48,49} for wave function. The second is the Feshbach projection approach for that the total Hamiltonian is projecting onto the discrete states of the scatterer subsystem. This procedure allows to formulate the Hamiltonian of the open quantum dot as the non-Hermitian Hamiltonian with complex eigenvalues.³⁷⁻⁴⁰ Then BIC appears for real eigenvalue of the effective Hamiltonian.^{7,9,12,18} Recently it was proven that both approaches to find BIC are equivalent.²⁴

For tight-binding modeling of quantum waveguide the formulation of the effective Hamiltonian is straightforward.^{43,44} However for the directed waveguide in PC there is a finite number of bands, N_W , while a number of hopping matrix elements is not restricted by only nearest neighbors as the case of the quantum waveguide. Therefore, the derivation of the effective Hamiltonian is not so simple task. Accordingly, based on the Ando's approach⁴⁶ we developed a different way to derive the effective Hamiltonian. The way is based on enlargement of the scattering region by addition of the buffer regions Ω_{CS} , where $C=L,R$ as shown in Fig. 1. The length of these regions is just the distance for which couplings of Wannier functions are relevant. The key point in our approach is the relations (22) which establish linear relations between amplitudes of incoming and reflected waves in the outside regions Ω_{CW} and the inside ones Ω_{CS} . As a result we obtain the relations (27) and (29) which, in turn, allow us to obtain an analog of the Lippman-Schwinger Eq. (33). The left-hand operator in the Lippman-Schwinger equation is just $H_{\text{eff}} - E$ for quantum mechanics. For PC case this operator is $H_{\text{eff}}(\omega)$ whose complex eigenvalues $z(\omega)$ are responsible for positions of resonances ω_m via the fix point equation $\text{Re}[z(\omega_m)] = 0$ and their widths $\Gamma_m = -2 \text{Im}[z(\omega_m)]$. Such a treatment of complex eigenvalues of

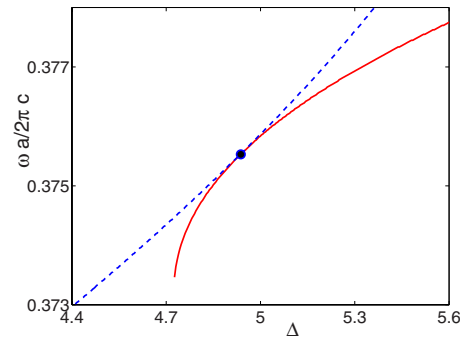


FIG. 7. (Color online) The maximal transmission of propagating photonic mode (dashed line) touches the line of the zero transmission (solid line) at the BIC point. The structure is similar to that as in Fig. 4(f) but the left defect rod has a radius $r_{\text{rod}} = 0.108a$. The dielectric constants of the defect rods were chosen as $\epsilon_1 = 5.5536 - \Delta/2$ and $\epsilon_2 = 5.5536 + \Delta/2$.

the effective Hamiltonian is justified for small resonance widths compared to their positions.³⁹

Because of interference of resonances caused by two defect rods it might happen that for some peculiar values of the dielectric constant ϵ_d of the defects one of the resonance width becomes zero while the other achieves maximum. For model case of two-level system coupled to waveguides such a case was established by Fan *et al.*¹¹ They derived the widths of the resonance states equal to zero for $kl=\pi(2n+1)$, $n=0,1,2,\dots$ for the even defects state and $kl=\pi 2n$, $n=1,2,\dots$ for the odd state correspondingly. Here l is a distance between the defect rods. It is worthy to note that our numerical computations of real system of pair defect rods in PC confirm these equations with high accuracy with slight deviation because of evanescent modes. It is clear that a

peculiar singular point of BIC cannot be achievable physically, at least, because of finite Q factor of the PC. However for the sufficiently high Q factor the Fano resonance width becomes very narrow as shown in Fig. 6. Moreover, the solution for transmission of photonic waves can be written in the form Eq. (39) in the vicinity of BIC. The coefficient α depends crucially on a path to the BIC point.^{14,18} In particular, one can always choose the paths in the space ϵ_d and ω to achieve that a contribution of BIC in the transport solution becomes dominant.

ACKNOWLEDGMENTS

We thank I. Rotter for helpful discussions.

-
- ¹J. von Neumann and E. Wigner, *Phys. Z.* **30**, 465 (1929).
²F. H. Stillinger and D. R. Herrick, *Phys. Rev. A* **11**, 446 (1975).
³F. H. Stillinger and T. A. Weber, *Phys. Rev. A* **10**, 1122 (1974).
⁴D. R. Herrick, *Physica B (Amsterdam)* **85**, 44 (1977).
⁵F. H. Stillinger, *Physica B (Amsterdam)* **85**, 270 (1977).
⁶F. Capasso, C. Sirtori, J. Faist, D. L. Sivco, S.-N. G. Chu, and A. Y. Cho, *Nature (London)* **358**, 565 (1992).
⁷H. Friedrich and D. Wintgen, *Phys. Rev. A* **32**, 3231 (1985).
⁸H. Friedrich and D. Wintgen, *Phys. Rev. A* **31**, 3964 (1985).
⁹T. V. Shahbazyan and M. E. Raikh, *Phys. Rev. B* **49**, 17 123 (1994).
¹⁰S. Fan, P. R. Villeneuve, J. D. Joannopoulos, and H. A. Haus, *Phys. Rev. Lett.* **80**, 960 (1998).
¹¹S. Fan, P. R. Villeneuve, J. D. Joannopoulos, M. J. Khan, C. Manolatou, and H. A. Haus, *Phys. Rev. B* **59**, 15882 (1999).
¹²A. Volya and V. Zelevinsky, *Phys. Rev. C* **67**, 054322 (2003).
¹³M. L. L. de Guevara, F. Claro, and P. A. Orellana, *Phys. Rev. B* **67**, 195335 (2003).
¹⁴A. F. Sadreev, E. N. Bulgakov, and I. Rotter, *Phys. Rev. B* **73**, 235342 (2006).
¹⁵C. S. Kim, A. M. Satanin, Y. S. Joe, and R. M. Cosby, *Phys. Rev. B* **60**, 10962 (1999).
¹⁶O. Olendski and L. Mikhailovska, *Phys. Rev. B* **66**, 035331 (2002).
¹⁷G. Ordonez, K. Na, and S. Kim, *Phys. Rev. A* **73**, 022113 (2006).
¹⁸E. N. Bulgakov, K. N. Pichugin, A. F. Sadreev, and I. Rotter, *JETP Lett.* **84**, 508 (2006).
¹⁹C. S. Kim and A. M. Satanin, *Phys. Rev. B* **58**, 15389 (1998).
²⁰I. Rotter and A. F. Sadreev, *Phys. Rev. E* **69**, 066201 (2004); **71**, 046204 (2005).
²¹A. F. Sadreev, E. N. Bulgakov, and I. Rotter, *JETP Lett.* **82**, 498 (2005).
²²D. C. Marinica, A. G. Borisov, and S. V. Shabanov, *Phys. Rev. Lett.* **100**, 183902 (2008).
²³C. Texier, *J. Phys. A* **35**, 3389 (2002).
²⁴E. N. Bulgakov, I. Rotter, and A. F. Sadreev, *Phys. Rev. A* **75**, 067401 (2007).
²⁵E. Yablonovitch, *Phys. Rev. Lett.* **58**, 2059 (1987).
²⁶S. John, *Phys. Rev. Lett.* **58**, 2486 (1987).
²⁷K. Busch, S. F. Mingaleev, A. Garcia-Martin, M. Schillinger, and D. Hermann, *J. Phys.: Condens. Matter* **15**, R1233 (2003).
²⁸L.-L. Lin, Z.-Y. Li, and B. Lin, *Phys. Rev. B* **72**, 165330 (2005).
²⁹J. Joannopoulos, R. D. Meade, and J. Winn, *Photonic Crystals* (Princeton University, Princeton, NJ, 1995).
³⁰E. Yablonovitch, T. J. Gmitter, R. D. Meade, A. M. Rappe, K. D. Brommer, and J. D. Joannopoulos, *Phys. Rev. Lett.* **67**, 3380 (1991).
³¹R. D. Meade, K. D. Brommer, A. M. Rappe, and J. D. Joannopoulos, *Phys. Rev. B* **44**, 13772 (1991).
³²S. L. McCall, P. M. Platzman, R. Dalichaouch, D. Smith, and S. Schultz, *Phys. Rev. Lett.* **67**, 2017 (1991).
³³Y. Xu, Y. Li, R. K. Lee, and A. Yariv, *Phys. Rev. E* **62**, 7389 (2000).
³⁴Z. Wang and S. Fan, *Phys. Rev. E* **68**, 066616 (2003).
³⁵S. Hughes, *Phys. Rev. Lett.* **98**, 083603 (2007).
³⁶N. Marzari and D. Vanderbilt, *Phys. Rev. B* **56**, 12847 (1997).
³⁷H. Feshbach, *Ann. Phys. (N.Y.)* **5**, 357 (1958); **19**, 287 (1962).
³⁸M. S. Livsic, *Sov. Phys. JETP* **4**, 91 (1957).
³⁹I. Rotter, *Rep. Prog. Phys.* **54**, 635 (1991).
⁴⁰F. M. Dittes, *Phys. Rep.* **339**, 215 (2000).
⁴¹J. Okořowicz, M. Płoszajczak, and I. Rotter, *Phys. Rep.* **374**, 271 (2003).
⁴²D. V. Savin, V. V. Sokolov, and H.-J. Sommers, *Phys. Rev. E* **67**, 026215 (2003).
⁴³S. Datta, *Electronic Transport in Mesoscopic Systems* (Cambridge University Press, Cambridge, England, 1995).
⁴⁴A. F. Sadreev and I. Rotter, *J. Phys. A* **36**, 11413 (2003).
⁴⁵H. Nakamura, N. Hatano, S. Garmon, and T. Petrosky, *Phys. Rev. Lett.* **99**, 210404 (2007).
⁴⁶T. Ando, *Phys. Rev. B* **44**, 8017 (1991).
⁴⁷A. Mekis, S. Fan, and J. D. Joannopoulos, *Phys. Rev. B* **58**, 4809 (1998).
⁴⁸M. Miyamoto, *Phys. Rev. A* **72**, 063405 (2005); *J. Math. Phys.* **47**, 082103 (2006).
⁴⁹S. Longhi, *Eur. Phys. J. B* **57**, 45 (2007); *Phys. Rev. B* **75**, 184306 (2007).